Coupling terahertz radiation between sub-wavelength metal-metal waveguides and free space using monolithically integrated horn antennae

J. Lloyd-Hughes, G. Scalari, A. van Kolck, M. Fischer, M. Beck and J. Faist

Institute for Quantum Electronics, ETH Zurich, 8092 Zurich, Switzerland

james.lloyd-hughes@phys.ethz.ch

Abstract: Broadband horn antennae are presented that efficiently couple terahertz radiation between sub-wavelength metal-metal waveguides and free space. Sub-picosecond terahertz pulses were coupled into and out from sub-wavelength parallel-plate waveguides by using the horn antennae in a terahertz time-domain spectrometer. Monolithic antennae were fabricated at the facets of metal-metal terahertz quantum cascade lasers, and laser action was observed for devices emitting at 1.4 THz, 2.3 THz and 3.2 THz. A good far-field laser radiation pattern (FWHM less than 11 °) is obtained as a result of the significant expansion of the optical mode by the antenna.

OCIS codes: (140.5965) Semiconductor lasers, quantum cascade, (300.6495) Spectroscopy, terahertz.

References and links

1. G. Scalari, C. Walther, M. Fischer, R. Terazzi, H. Beere, D. Ritchie, and J. Faist, "THz and sub-THz quantum cascade lasers," Laser Photon. Rev. **3**, 45–66 (2009).
2. A. J. L. Adam, I. Kasalynas, J. N. Hovenier, T. O. Klaassen, J. R. Gao, E. E. Orlova, B. S. Williams, S. Kumar, Q. Hu, and J. L. Reno, "Beam patterns of terahertz quantum cascade lasers with subwavelength cavity dimensions," Appl. Phys. Lett. **88**, 151,105 (2006).
3. S. Kohen, B. S. Williams, and Q. Hu, "Electromagnetic modeling of terahertz quantum cascade laser waveguides and resonators," J. Appl. Phys. **97**, 053,106 (2005).
4. M. I. Amanti, M. Fischer, C. Walther, G. Scalari, and J. Faist, "Horn antennas for terahertz quantum cascade lasers," Electron. Lett. **43**, 573–574 (2007).
5. W. Maineult, P. Gellie, A. Andronico, P. Filloux, G. Leo, C. Sirtori, S. Barbieri, E. Peytavit, T. Akalin, J. F. Lampin, H. E. Beere, and D. A. Ritchie, "Metal-metal terahertz quantum cascade laser with micro-transverse-electromagnetic-horn antenna," Appl. Phys. Lett. **93**, 183,508 (2008).
6. A. W. M. Lee, Q. Qin, S. Kumar, B. S. Williams, Q. Hu, and J. L. Reno, "High-power and high-temperature THz quantum-cascade lasers based on lens-coupled metal-metal waveguides," Opt. Lett. **32**, 2840–2842 (2007).
7. M. I. Amanti, M. Fischer, G. Scalari, M. Beck, and J. Faist, "Low divergence single-mode terahertz quantum cascade laser," Nature Photonics; advance online publication (DOI 10.1038/NPHOTON.2009.168) (2009).
8. Y. Chassagneux, R. Colombelli, W. Maineult, S. Barbieri, H. E. Beere, D. A. Ritchie, S. P. Khanna, E. H. Linfield, and A. G. Davies, "Electrically pumped photonic-crystal terahertz lasers controlled by boundary conditions," Nature **457**, 174–178 (2009).
9. N. F. Yu, J. Fan, Q. J. Wang, C. Pflugl, L. Diehl, T. Edamura, M. Yamanishi, H. Kan, and F. Capasso, "Small-divergence semiconductor lasers by plasmonic collimation," Nat. Photonics **2**, 564–570 (2008).
10. C. A. Schmuttenmaer, "Exploring dynamics in the far-infrared with terahertz spectroscopy," Chem. Rev. **104**, 1759–1779 (2004).
11. R. Mendis and D. Grischkowsky, "Undistorted guided-wave propagation of subpicosecond terahertz pulses," Opt. Lett. **26**, 846–848 (2001).

#116506 - $15.00 USD Received 31 Aug 2009; revised 23 Sep 2009; accepted 23 Sep 2009; published 25 Sep 2009

12. G. Gallot, S. P. Jamison, R. W. McGowan, and D. Grischkowsky, "Terahertz waveguides," J. Opt. Soc. Am. B-Opt. Phys. **17**, 851–863 (2000).
13. E. Rosencher and B. Vinter, *Optoelectronics*, 1st ed. (Cambridge University Press, 2002).
14. M. I. Amanti, G. Scalari, R. Terazzi, M. Fischer, M. Beck, and J. Faist, "Bound-to-continuum terahertz quantum cascade laser with a single quantum well phonon extraction/injection stage," To appear in New. J. Phys. (2009).
15. C. Walther, M. Fischer, G. Scalari, R. Terazzi, N. Hoyler, and J. Faist, "Quantum cascade lasers operating from 1.2 to 1.6 THz," Appl. Phys. Lett. **91**, 131,122 (2007).

1. Introduction

Recent years have seen marked improvements in the temperature performance and frequency range of terahertz quantum cascade lasers (THz QCLs), with the best performance achieved utilizing metal-metal waveguides [1]. Here, the TM-polarized laser mode is contained vertically within the active region by a parallel-plate waveguide, and lateral mode confinement is obtained by etching a ridge. While providing good mode overlap with the active region, metal-metal waveguides typically suffer from widely divergent beam patterns [2] owing to the significant diffraction from their facets, which have a sub-wavelength height ($\sim 10\,\mu$m compared to free space wavelengths of $\sim 70-250\,\mu$m). The facet reflectivity is also high [3], typically greater than 70 %, limiting the output power of the laser. A number of solutions to these problems have been proposed, including placing metallic horn antennas on top of the metal-metal waveguide [4, 5], locating silicon lenses on the facets [6] or engineering the far-field using third-order distributed feedback gratings [7], 2D photonic bandgap structures [8] or plasmonic gratings [9]. However, these approaches are typically mechanically unstable, technologically challenging, and require extra components. In addition some of these solutions only work at specific frequencies and are unsuitable for broadband radiation coupling.

In this article we report a straightforward and mechanically robust method of coupling terahertz radiation out from and into sub-wavelength metal-metal waveguides, using horn antennae fabricated 'on-chip'. Broadband pulses of THz radiation were coupled into sub-wavelength waveguides using the horn antennae in a THz time-domain spectrometer. Finite-difference time-domain simulations were employed to elucidate the effects of the antenna structure on the broadband THz pulse. The demonstrated coupling principle is then applied to active devices by integrating horn antennae directly inside the metal-metal waveguide of THz QCLs emitting at different frequencies. Laser action is obtained at 3.2 THz with a narrow far-field beam pattern. By additionally demonstrating lasers with integrated horn antennae operating at 2.3 THz and 1.4 THz we show that this concept provides a broadband impedance coupling solution for THz QCLs.

2. Horn fabrication

Quantum cascade structures were grown by molecular beam epitaxy on $Al_{0.5}Ga_{0.5}As$ etch-stop layers on top of semi-insulating GaAs substrates. Samples were Au-Au thermocompression wafer-bonded to an n^+ GaAs wafer for mechanical support, before the semi-insulating substrate was polished to a thickness of $\sim 200\,\mu$m. The horn antenna was then defined from the semi-insulating GaAs substrate using standard photolithography and wet etching techniques. The structure is shown schematically in Fig. 1(a), and an image of a typical device is shown in Fig. 1(b).

The etching of the horn was performed using an H_2SO_4:H_2O_2:H_2O etchant (1:8:1 volume ratio) for the first half of the horn's height, before switching to a selective etchant (citric acid and H_2O_2) that stops on the $Al_{0.5}Ga_{0.5}As$ layer. The horn's profile was measured with a surface profilometer [Fig. 1(c)] and flares from 27° at the base to 48° at the top of the horn. The changing slope results from the different etch rate of the two etchants, and helps to expand

#116506 - $15.00 USD Received 31 Aug 2009; revised 23 Sep 2009; accepted 23 Sep 2009; published 25 Sep 2009

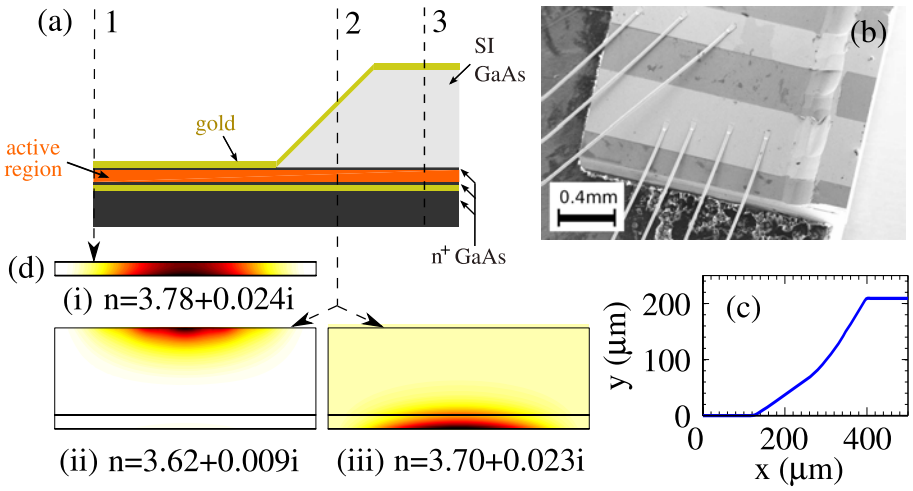

Fig. 1. (a) Schematic cross-section and (b) electron micrograph of a semi-insulating GaAs horn antenna integrated into a metal-metal terahertz quantum cascade laser. The vertical axis in (a) is the growth direction and the horizontal is the light propagation direction. The layers in (a) are, from bottom to top at the right hand side: n^+ substrate, gold, n^+ GaAs contact, active region, n^+ GaAs contact, semi-insulating GaAs horn, gold. (c) Measured profile of horn. (d) Calculated intensities of low-loss eigenmodes at 3.0 THz at the cross-sections shown in (a). For cross-section 1, through the active region, the waveguide is 300 μm wide and 12 μm high, and the mode intensity is shown in (i). For cross-section 2, in the flared part of the horn (where the undoped GaAs is 100 μm high), eigenmodes are bound to the top (ii) or bottom (iii) metal. The actual mode will be a combination of the two.

the optical mode quasi-adiabatically from the active region (height $h = 12.0\,\mu$m) to a size of $H = 210\,\mu$m. A second photolithography and wet-etching step defined ridges (200-350 μm wide), and finally a Ti/Au top contact was deposited on the ridge and the horn. The end facets were defined by either cleaving along the top of the horn or across the metal-metal ridge, at position 3 or 1 in Fig. 1(a) respectively. Thus, devices with integrated horn antennae on one or both facets were produced.

3. Transmission of pulses of terahertz radiation

In order to test the propagation of terahertz radiation through the waveguide we performed transmission measurements (using terahertz time-domain spectroscopy [10], or THz-TDS) on test structures with two horns [Fig. 2(a)]. A 2.0 mm long double-sided horn antenna was fabricated from semi-insulating GaAs, using the sulfuric acid etchant described above. The height of the horn antennae were $H = 300\,\mu$m, and the height of the narrow section was $h = 35\,\mu$m. A reference sample was formed from a 2.0 mm long section of gold-coated n^+ GaAs with a 300 μm air gap. The incident electric field E_y was linearly polarized perpendicular to the plane of the substrate, as indicated in Fig. 2(a). Measurements were performed in a nitrogen purged chamber.

The time-domain pulses of terahertz radiation transmitted through the reference and the horn structure are reported in Fig. 2(b), and their amplitude spectra are shown in Fig. 2(c). In the time-domain the reference electric field is single-cycle because terahertz pulses can propagate freely in parallel-plate waveguides in the TEM mode, which exhibits low loss and minimal group velocity dispersion [11]. In contrast the pulse through the horn antenna exhibits a num-

#116506 - $15.00 USD Received 31 Aug 2009; revised 23 Sep 2009; accepted 23 Sep 2009; published 25 Sep 2009

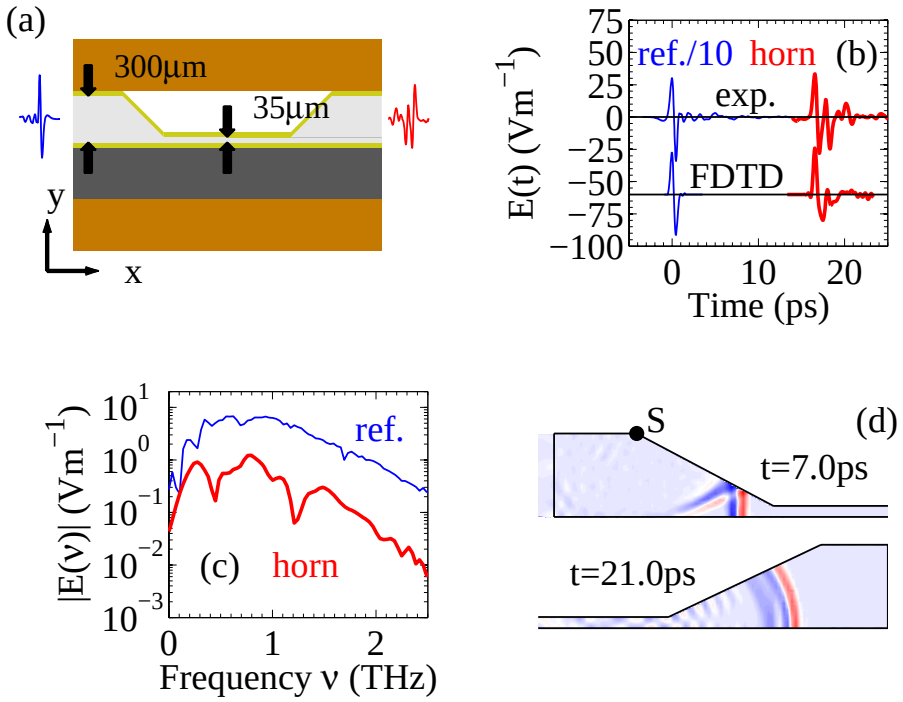

Fig. 2. (a) In the transmission measurements terahertz pulses propagated in the x-direction, and were linearly polarized in the y-direction. The layers are (from bottom to top) copper, n^+ GaAs substrate, gold, semi-insulating GaAs, gold, copper. (b) Measured electric field E_y transmitted through the reference waveguide (divided by 10) and through the horn antenna sample (top two lines). Below are FDTD simulations of E_y. (c) Electric field amplitude spectra of the pulses through the reference and horn antenna. (d) Finite-difference time-domain simulations of E_y at times of 7.0 ps and 21.0 ps after the injection of a single-cycle pulse into the waveguide at the left facet (regions with positive E_y are red, and negative are blue). Point S is the source of a secondary wavefront.

ber of cycles, and the amplitude of the transmitted electric-field is about 10 % of the reference across a broad frequency range ($0.2-2.5$ THz, or $1500-120\,\mu$m in wavelength). The change in spectral amplitude around 1.2 THz visible in Fig. 2(c) may originate from the cut-off frequency of the TM_1 mode [11, 12], which is at $f = c/2hn = 1.2$ THz for $h = 35\,\mu$m and $n = 3.6$. The ratio λ/h for the lowest frequency (0.2 THz) corresponds to 43 using the vacuum wavelength (1500 μm) and 12 using the wavelength in GaAs (418 μm), illustrating that highly sub-wavelength coupling is achievable using this scheme, an advantage over diffraction-limited approaches such as silicon lenses.

In order to understand the origin of the apparent dispersion of the terahertz pulse in the horn antenna waveguide we performed finite difference time-domain (FDTD) simulations of the pulse's propagation through the structure, using the exact dimensions of the waveguide. A single-cycle pulse with a bandwidth comparable to that of the experiment is injected into the left facet of the waveguide at zero time. Figure 2(d) indicates the pulse shape 7.0 ps later, when the positive peak of E_y (red) has almost reached the 35 μm section. The secondary wavefronts trailing the pulse are generated by the change in gradient at the start of the horn's slope (point S), and arrive later in time due to the extra path length traveled. At a time of 21.0 ps the pulse has

#116506 - $15.00 USD Received 31 Aug 2009; revised 23 Sep 2009; accepted 23 Sep 2009; published 25 Sep 2009

reached the second horn antenna, and the secondary wavefronts remain visible. Upon coupling into free-space these create the oscillations visible in the time-domain after the initial pulse [Fig. 2(b)]. This alteration of the phase of the wavefront means that light making one complete round-trip of the waveguide will not satisfy the phase condition for laser action [13]. The shape of the simulated pulse is in reasonable agreement with the experiment [Fig. 2(b)]; the differences may arise from neglecting the roughness of the waveguide and/or the dispersion of the refractive index in semi-insulating GaAs.

The power reflected at the boundary between the narrow ridge section and the horn antenna was also estimated from the FDTD simulations. At 1.5 THz the power reflectivity upon propagation from $h = 35\,\mu$m to $H = 300\,\mu$m section is 15 %. The reflectivity from a waveguide with $h = 12\,\mu$m and $H = 200\,\mu$m is 16 % at 1.5 THz, and 33 % at 3.0 THz. These values are much lower than the typical facet reflectivities between a metal-metal waveguide and free space [3], where the reflectivity is about 75 % at 3.0 THz and 90 % at 1.5 THz. The reflectivity for the cleaved facets (GaAs/air) is close to 30 %, as in a single-plasmon waveguide [3].

The propagation of light in the laser waveguides will be modified by the presence of the two doped contact layers. Figure 1(d) shows 2D simulations at 3.0 THz of the eigenmodes at different cross-sections through the device [shown in (a)]. The complex refractive index of the active region and horn was taken to be that of semi-insulating GaAs, measured at room temperature using THz-TDS to be $n = 3.63 + 0.008i$. For the doped contact layers the refractive index was calculated from that of a free electron gas. In the metal-metal waveguide section [height 12 μm and width 300 μm] the mode is tightly confined within the active region, with laser action on the lowest loss (the TEM) mode, which has an effective index $n = 3.78 + 0.024i$. When the height of the semi-insulating GaAs region has reached 100 μm eigenmodes exist that are bound to either the active region ($n = 3.70 + 0.023i$, note the similarity to the single-plasmon waveguide) or the top metal ($n = 3.62 + 0.009i$). Away from metal-metal section, light will only be amplified if there is good overlap with the active region, and if the active region retains the correct electrical bias. The lower refractive index of the mode bound to the top metal compensates slightly for the phase distortion of the wavefront, discussed above.

4. Laser emission

The horn antenna devices were characterized in pulsed mode (5 % duty cycle) in a helium flow cryostat at 10 K, and the emitted light was detected with a calibrated absolute power meter. Spectra were recorded with a home-built vacuum FTIR with a resolution of 15 GHz. In Fig. 3(a) laser action is reported for a 3.2 THz QCL with a horn antenna integrated onto one facet (solid line) and with horns on both facets (dashed line). The bandstructure of the active region was a four quantum well design with a phonon depopulation well [14]. The ridges were 300 μm wide and 1.9 mm long, and the total length of each horn section was 550 μm. Current densities were calculated using the length of the ridge, i.e. assuming the horn sections do not contribute to laser action. The threshold current density J_{thr} increases from 375 Acm^{-2} for the single horn antenna to 440 Acm^{-2} for a double horn antenna, and the maximum output power was over 20 mW in both cases. For a comparable metal-metal ridge waveguide $J_{\mathrm{thr}} = 250\ \mathrm{Acm}^{-2}$ and the maximum power is < 5 mW. The rise in J_{thr} with an extra horn antenna results from the reduced reflectivity of the facet (discussed above), raising the mirror losses of the cavity [3].

The spectra shown in Fig. 3(b) indicate that the laser remains single mode from laser threshold to maximum output power, and that the lasing transition does not substantially Stark shift with voltage. This is a consequence of the shallow ridge etch used (2.0 μm), which creates a high loss for the high-order lateral modes of the waveguide. Laser action on different longitudinal modes is not possible because of the wavefront distortion discussed above.

Horn antennae were also fabricated on epilayers that lase in standard metal-metal waveg-

#116506 - $15.00 USD Received 31 Aug 2009; revised 23 Sep 2009; accepted 23 Sep 2009; published 25 Sep 2009

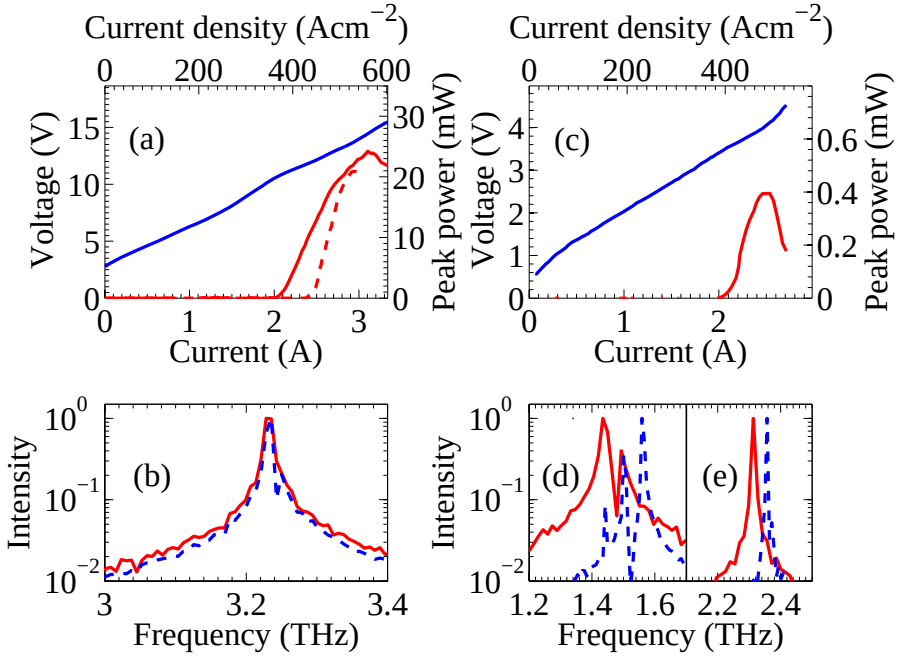

Fig. 3. (a) Light-current-voltage characteristics at 10 K for a 3.2 THz QCL with an integrated horn antenna on one facet (solid lines) or both facets (dashed lines). (b) Spectra for the double-sided horn device are shown on a logarithmic scale at laser threshold (solid line) and at the maximum current (dashed line). (c) and (d) are similar graphs for a 1.4 THz QCL with a horn antenna on one facet. (e) The spectra at threshold of a 2.3 THz QCL in a metal-metal waveguide (solid line) and with a single integrated horn (dashed line).

uides in the range 1.34-1.58 THz (a split-injector, bound-to-continuum design [15]) and 2.27-2.37 THz (a phonon depopulation design rescaled from the 3.2 THz design). The current-voltage characteristics of the low-frequency QCL with a single horn antenna are reported in Fig. 3(c), and the spectra measured at threshold and maximum current are shown in Fig. 3(d). Laser action is obtained from 1.44 THz to 1.56 THz, with a reduced frequency range in comparison to the metal-metal waveguide as a result of the lower facet reflectivity. The laser frequency is widely tunable via the quantum-confined Stark effect as the intersubband transition is diagonal [15]. The 2.3 THz horn structure also started lasing at a higher frequency than in a metal-metal waveguide [Fig. 3(e)]. Devices with horn antennae on both facets did not lase. In a metal-metal waveguide the current density required for emission at 1.44 THz is 360 Acm^{-2}, and for 1.56 THz it is 426 Acm^{-2}. This is in agreement with the values for the horn device (376 Acm^{-2}, 460 Acm^{-2}) when the length of the ridge (1.36 mm) is used, indicating that no current flows in the horn sections.

The angular emission pattern of the 3.2 THz horn antenna laser was measured using a pyroelectric detector mounted on a two-axis rotation stage, and is reported in Fig. 4. The observed emission pattern is narrow, with a full-width-half-maximum of 11 $^\circ$ in the growth direction (θ) and 4 $^\circ$ in the plane of the device (ψ). For this device the extent of the beam in the ψ directions was controlled by flaring the gold top contact from 300 μm width on the ridge to 500 μm on top of the horn. The emission pattern of the lower frequency lasers was not measured due to their lower power (0.4 mW for the 1.4 THz design).

#116506 - $15.00 USD Received 31 Aug 2009; revised 23 Sep 2009; accepted 23 Sep 2009; published 25 Sep 2009

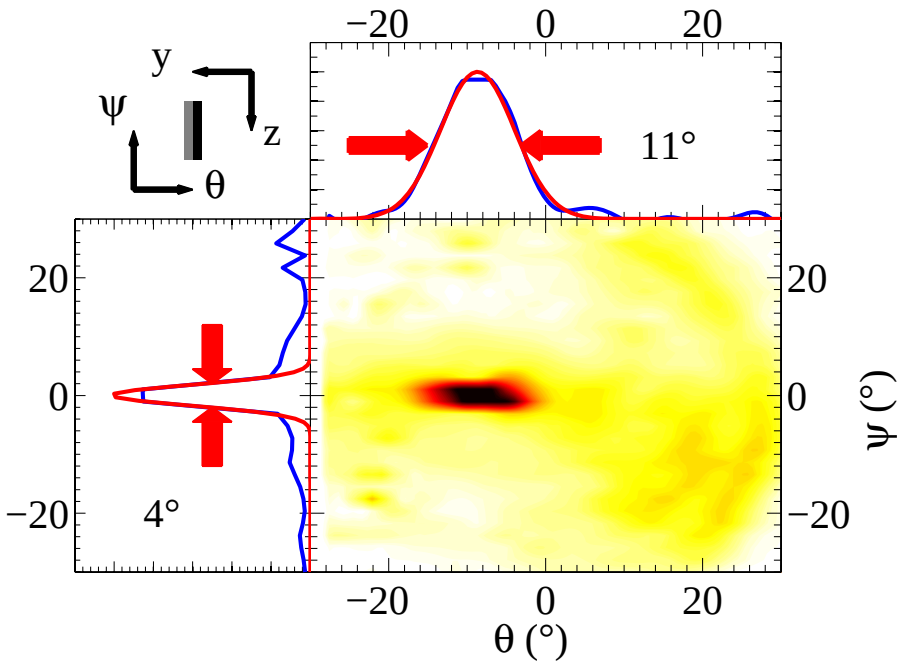

Fig. 4. Far-field emission pattern of a 3.2 THz laser with an integrated horn antenna. The θ-axis is parallel to the growth direction (y-axis), and the ψ-axis is perpendicular to it, as indicated in the cartoon in the top left corner, which looks at the horn antenna edge-on. The cross-sections of the far field emission pattern (top and left sub-plots) show the measured power (blue lines) and a Gaussian fit (red lines).

5. Conclusion

In conclusion, horn antennae were fabricated at the ends of metal-metal waveguides by combining wafer bonding with wet etching. Such structures were then integrated on active devices by realizing metal-metal THz quantum cascade lasers. The horn antennae raised the threshold for laser action as a result of lowering the facet reflectivity, and produced a good far-field radiation pattern. The narrow beam diameter in comparison to metal-metal waveguides makes lasers with integrated horn antennae suitable for use in spectroscopy and imaging applications. In addition, the presented horn antennae may find use in widely tunable external cavity lasers and broadband THz amplifiers.

Acknowledgements

The authors would like to thank M. I. Amanti for technical assistance. This work was supported by the Swiss National Science Foundation and the Marie-Curie Training Network POISE.

#116506 - $15.00 USD Received 31 Aug 2009; revised 23 Sep 2009; accepted 23 Sep 2009; published 25 Sep 2009